



A hybrid catalyst for decontamination of organic pollutants based on a bifunctional dicopper(II) complex anchored over niobium oxyhydroxide



Tamyris T. da Cunha^a, Talita E. de Souza^a, Wallace D. do Pim^{a,b}, Leandro D. de Almeida^a, Gustavo M. do Nascimento^c, Enrique García-España^d, Mario Inclán^d, Miguel Julve^d, Humberto O. Stumpf^a, Luiz C.A. Oliveira^a, Cynthia L.M. Pereira^{a,*}

^a Departamento de Química, ICEX, Universidade Federal de Minas Gerais, 31270-901, Belo Horizonte, MG, Brazil

^b Departamento de Química, Centro Federal de Educação Tecnológica de Minas Gerais, 30421-169 Belo Horizonte, MG, Brazil

^c Centro de Ciências Naturais e Humanas (CCNH), Universidade Federal do ABC, 09210-580 Santo André, SP, Brazil

^d Departament de Química Inorgànica, Institut de Ciència Molecular (ICMol), Universitat de València, C/Catedrático José Beltrán 2, 46980 Paterna, València, Spain

ARTICLE INFO

Article history:

Received 21 July 2016

Received in revised form 26 January 2017

Accepted 31 January 2017

Available online 8 February 2017

Keywords:

Niobium oxyhydroxide

Copper(II) complex

Hybrid-catalyst

Photocatalysis

ABSTRACT

This article describes the preparation and characterization of a hybrid oxidation catalyst for decontamination of organic pollutants which involves a bifunctional dicopper(II) complex and the niobium(V) oxyhydroxide as the active species, the later one being also a solid support. The pH range for the existence of the active species was determined by potentiometric and UV-vis spectroscopy at 25 °C and 0.15 M NaCl in a H₂O/EtOH (70:30 v/v) solvent mixture containing copper(II) and the ligand N,Ni-2,2'-ethylenediphenylenebis(oxamic acid) (H₄L). As far as the hybrid material is concerned, FTIR, FT-Raman, TEM and SEM images, surface area and TG/DTA analyses showed the occurrence of a chemical interaction between the dicopper(II) complex and the surface hydroxo groups of the niobium oxyhydroxide whereas ESI-MS and UV-vis spectroscopy evidence a total disappearance of the signals due to the organic dye which is used as model molecule. This hybrid material seems to combine the different properties of the components increasing its catalytic activity for oxidizing organic pollutants at different pH values.

© 2017 Elsevier B.V. All rights reserved.

1. Introduction

The term “hybrid catalyst” is used to describe a type of tailor-made materials involving the intentional combination of different existing compounds or composites to achieve the superposition of their catalytic properties [1]. In this context, the choice of a series of matrices as support is based on their high surface area, for instance activated charcoal and mesoporous silica [2]. Hybrid catalysts arise from the immobilization of active metal complexes, organometallic compounds or enzymes on a solid support, which eventually makes possible an ease separation after the end of the desired catalysed reaction [3]. Metal oxides that exhibit catalytic activity are even more promising to be used as supports, since the combination of the two catalysts can bring significant results in order to

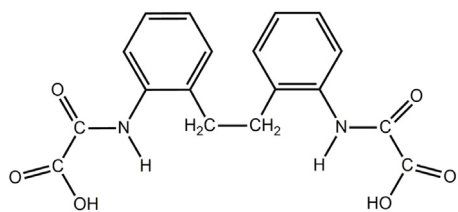
improve the catalytic activity and the reuse of the catalyst [4]. In this respect, the development of new niobium-based hybrid catalysts is particularly promising, because their oxides have acid sites which allow their application as catalysts in several reactions such as hydration [5] or condensation [6] and also in advanced oxidation processes [7]. Another aspect that constitutes an extra motivation in our investigation on the chemistry of niobium is that the mining availability of the niobium-based compounds and composites in Brazil corresponds to approximately 98% of worldwide mining of its ores, particularly in the state of Minas Gerais [8].

Among all the niobium-based catalysts such as Nb₂O₅ [9], polyoxoniobates [10] and organometallic complexes [11], the oxyhydroxide family is in the spotlight [12–15]. This obeys in part the possibility of a selective interaction between the surface hydroxo groups and the oxygen or nitrogen atoms from the organic ligands of a metallorganic complex by hydrogen bonding to form a hybrid catalyst with a decreased leaching of the metal complex [16].

Having in mind the diversity of hybrid materials containing a surface supported metallorganic complex, the functionalized

* Corresponding author.

E-mail addresses: cynthialopes@ufmg.br, lopecsynthia@yahoo.com.br (C.L.M. Pereira).



Scheme 1. Structural formula of H_4L .

oxamate ligands open a window for a new class of complexes anchored at the niobium(V) oxyhydroxide support. Restricting ourselves to the field of catalysis, an oxamate-containing dicopper(II) complex with the flexible N,N' -2,2'-ethylenediphenylenebis(oxamic acid) as ligand (H_4L , see **Scheme 1**) has shown a unique stimuli-responsive multifunctional behaviour affording a molecular switch based on the variation of the pH in heterogeneous phase. The H_4L molecule as well as its deprotonated forms can adopt the antiperiplanar ($\text{H}_4\text{L}^{\text{anti}}$) or gauche ($\text{H}_4\text{L}^{\text{gauche}}$) conformations by a free rotation of the single carbon–carbon bond which is triggered by a pH variation [17].

That being so, two dicopper(II) species of formula $(n\text{-Bu}_4\text{N})_4[\text{Cu}_2(\text{L}^{\text{gauche}})_2]\cdot 4\text{H}_2\text{O}$ ($n\text{-Bu}_4\text{N}^+$ = tetra-*n*-butylammonium cation) and $[\text{Cu}_2(\text{H}_2\text{L}^{\text{anti}})_2](\text{EtOH})_2\cdot 2\text{EtOH}$ have been previously isolated and structurally characterized [17]. As far as we are aware, other complexes containing the neutral tetra- (H_4L) or triprotic (H_3L^-) derivatives as ligands are unknown.

In this contribution, we focus on the preparation of a hybrid redox catalyst for decontamination of organic pollutants and on its characterization by TEM and SEM images as well as surface area analysis. We evaluate the interactions between the niobium(V) oxyhydroxide, $\text{NbO}_2(\text{OH})$ (**1**), and the above mentioned oxamate-containing dicopper(II) complexes (abbreviated hereafter as $[\text{Cu}_2(\text{H}_2\text{L})_2]$ and $[\text{Cu}_2\text{L}_2]^{4-}$) by means of the FTIR and FT-Raman vibrational spectroscopies. These dicopper(II) complexes are resistant under wide pH ranges without undergoing any decomposition such as demetallation or precipitation of copper(II) hydroxide, as shown by potentiometric and UV-vis measurements. We investigated the complex formation between copper(II) and H_4L in solution as a function of the pH envisaging a better understanding of the possible interaction between the two counterparts of the hybrid catalyst.

2. Experimental

2.1. Materials

The niobium(V) oxyhydroxide $\text{NbO}_2(\text{OH})$ (**1**) used as matrix, the complex $(n\text{-Bu}_4\text{N})_4[\text{Cu}_2\text{L}_2]$ ($n\text{-Bu}_4\text{N}^+$ = tetra-*n*-butylammonium) and the $\text{K}_2\text{H}_2\text{L}$ salt were synthesized as reported in the literature [12,13,17,18]. The hybrid catalyst $\text{NbO}_2(\text{OH})\text{-}[\text{Cu}_2\text{L}_2]$ (**2a**) was prepared as follows: 1.728 g of **1** was added to a solution containing 150 mg of $(n\text{-Bu}_4\text{N})_4[\text{Cu}_2\text{L}_2]$ in 70 mL of water under continuous stirring. The resultant dispersion was refluxed at 100 °C for 90 min, a colour change from green to blue being observed after this temperature was reached. After 1 h, the suspension obtained was placed on a hot plate at 60 °C for one week resulting in a sky blue material. Yield: 1.757 g, 93.6%.

2.2. Physical techniques

Thermogravimetric analyses (TG/DTA) were performed with a Shimadzu TGA50H by using approximately 2.0 mg of each sample packed into an alumina crucible. The samples were heated at

10 °C min⁻¹ from room temperature to 700 °C in a dynamic flow of air (flow rate of 100 cm³ min⁻¹).

The IR spectra were recorded with a Perkin Elmer FTIR RXI spectrometer in the range 4000–400 cm⁻¹ by using KBr pellets and an average of 64 scans with a resolution of 4 cm⁻¹. UV-vis measurements were carried out with a UV-vis 2600 Shimadzu in the wavelength range 280–800 nm. A MultiRAM FT-Raman Bruker spectrometer with the 1064.0 nm laser line from an air-cooled diode-pumped Nd:YAG laser was used to get the Fourier transform Raman (FT-Raman) spectra of the solid samples. The calibration of the equipment (wavenumbers and intensities of the peaks) was performed by using a standard Nylon sample. Experiments were performed under room conditions with a backscattering geometry. The laser beam with approximately 1 mm spot (the largest spot available) was focused on the centre of the aluminum disk (using the laser guided of the FT-Raman as reference) containing the sample at the front compartment by means of a 20 mW laser power.

X-ray powder diffraction patterns were obtained at room temperature by using a Rigaku/Geirgflex diffractometer. Data were collected in the Bragg/Brentano mode (1° s⁻¹) by using monochromatic Cu-K α radiation ($\lambda = 1.542 \text{ \AA}$).

Electrospray ionization mass spectrometry ESI-MS was performed with an ION-TRAP LCQFleet (ThermoScientific) mass spectrometer in positive mode to evaluate the oxidation of methylene blue dye. The reaction samples were analyzed by introducing aliquots into the ESI source with a syringe pump at a flow rate of 15 L min⁻¹. The spectral data obtained were averaged for five scans at 0.2 s each one. Typical ESI conditions used a heated capillary temperature of 275 °C, sheath gas (N₂) at a flow rate of 15 units (ca. 4 L min⁻¹), a spray voltage of 2 kV, and capillary and tube lens offset voltages of 25 V.

HR-ESI mass spectra of a solution water/methanol 70:30 v/v solutions containing $\text{K}_2\text{H}_2\text{L}$ and $[\text{Cu}(\text{H}_2\text{O})_6(\text{ClO}_4)_2]\cdot 6$ in a 1:1 molar ratio were acquired in the positive ion mode using a Triple TOF 5600 hybrid quadrupole time-of-flight (TOF) mass spectrometer. N₂ was used as a curtain and nebulizing gas. The experiments were performed at a voltage of 5300 V and GS1 and GS2 (35 ψ) ion source gas at 723.15 K. The AB SCIEX Peak View software was used for the analysis of the data.

Transmission electron microscopy (TEM) images were obtained by means of a Tecnai G2 200 kVSEI microscope. The samples were suspended in acetone and deposited onto a holey carbon film on 200 mesh copper grids. Scanning electron microscopy images were obtained by using a FEG – Quanta 200 FEI microscope. The samples were suspended in acetone and deposited onto silicon chip specimen support.

2.3. Electromotive force measurements and UV-vis titrations

The potentiometric titrations were carried out in a water/ethanol 70:30 (v/v) mixture at 298.1 ± 0.1 K using 0.15 M NaCl as the supporting electrolyte. The experimental procedure (buret, potentiometer, cell, stirrer, micro-computer, etc) has been fully described elsewhere [19]. The acquisition of the emf data was performed with the computer program PASAT [20]. The reference electrode was an Ag/AgCl electrode in saturated KCl solution. The glass electrode was calibrated as a hydrogen ion concentration probe by titration of previously standardized amounts of HCl with CO₂-free water/ethanol 70:30 (v/v) NaOH solutions. The equivalence point was calculated by the Gran's method [21,22], which gives the standard potential (E°) and the ionic product of water [$\log K_w = 14.16(1)$ in 70:30 water/ethanol] [23]. The computer program HYPERQUAD was used to calculate the protonation and stability constants [24]. The pH range investigated ($\text{pH} = -\log [\text{H}^+]$)

Table 1

Cumulative protonation or stability constants, determined at 298 K with 0.15 M NaCl in H₂O/EtOH (70:30 v/v) by UV-vis or potentiometric titration.

Reaction	$\log \beta^a$
H ₂ L ²⁻ + 2H ⁺ ⇌ H ₄ L	4.66(1) ^b
H ₂ L ²⁻ + H ⁺ ⇌ H ₃ L ⁻	2.80(1) ^c
H ₂ L ²⁻ + Cu ²⁺ ⇌ [Cu(H ₂ L)]	3.8(1) ^c
2H ₂ L ²⁻ + 2Cu ²⁺ ⇌ [Cu ₂ (H ₂ L) ₂]	10.8(1) ^c
2H ₂ L ²⁻ + 2Cu ²⁺ ⇌ [Cu ₂ (H ₂ L) ₂] ²⁻ + 2H ⁺	-0.3(1) ^c
2H ₂ L ²⁻ + 2Cu ²⁺ ⇌ [Cu ₂ (HL)L] ³⁻ + 3H ⁺	-8.3(1) ^c
2H ₂ L ²⁻ + 2Cu ²⁺ ⇌ [Cu ₂ L ₂] ⁴⁻ + 4H ⁺	-17.3(1) ^c

^a Values in parentheses correspond to the standard deviation in the last significant digit.

^b By UV-vis titration.

^c By potentiometric titrations.

was 2.5–11.0. The different titration curves were treated as separate curves without significant variations in the values of the stability constants. Finally, the sets of data were merged together and treated simultaneously to give the final stability constants.

K₂H₂L and [Cu(H₂O)₆](ClO₄)₂ solutions were prepared in a water/ethanol 70:30 (v/v) mixture with 0.15 M NaCl as background electrolyte. Absorption spectra were recorded at variable pH values measured. Adjustments of the hydrogen ion concentration of the solutions were made with diluted HCl and NaOH solutions. The computer program HypSpec was used to calculate the values of the stability constants from the spectroscopic data [24].

2.4. Catalytic tests

Fenton-like catalytic tests were carried out by using a solution of methylene blue (MB) dye (100 ppm) and H₂O₂ (50%, 50 mL) and the hybrid material **2a** (10 mg) with continuous stirring and in the dark. A blank test with only **1** in the same conditions was done for comparison.

The reuses of the catalysts were analyzed by means of Fenton reactions at each 30 min and for 5 times, with the replacement with a new solution each 30 min. After this time, the resultant mixture was centrifuged, the catalyst was separated and a new solution was added in the same conditions without washing the catalyst. This reuse was analyzed by ESI-MS spectrometry and UV-vis in the range 280–800 nm.

Dibenzothiophene (DBT) oxidation tests were also performed by the Fenton-like reaction using 1000 ppm solution of DBT in *n*-hexane, H₂O₂ (50%, 1 mL) and 10 mg of **2a**. The tests were carried out under three different types of radiation (artificial UV and visible and ambient light) with continuous stirring for 60 min. The absorption of DBT was monitored with a UV-vis spectrophotometer ($\lambda_{\text{max}} = 236$ nm).

3. Results and discussion

3.1. Electromotive force measurements

The protonation constants of H₂L²⁻ and the stability constants of its copper(II) complexes determined by electromotive force measurements and UV-vis titrations, are included in Table 1.

From the four expected protonation steps of the free ligand (L⁴⁻), only one corresponding to the protonation of one of the carboxylate groups could be identified by potentiometric titration in the explored pH range 2.5–11.0 [$pK_{a2} = 2.80(1)$]. For determining the protonation constant of the second carboxylate group, which would occur at a more acidic pH, a UV-vis pH titration of a 4×10^{-5} M ligand solution was performed in the pH range 0.8–4.1 (Fig. S1, ESI). Treatment of these spectroscopic data by using a nonlinear fitting software [24], gave a value of 1.86(1) logarithmic units (pK_{a1}) corresponding to the protonation of the second

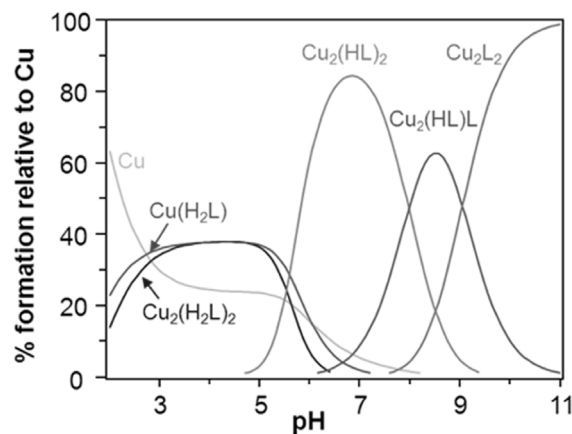


Fig. 1. Distribution diagram for the system Cu²⁺- L⁴⁻ ([Cu²⁺]=[L⁴⁻]=1×10⁻³ M, H₂O/EtOH (70:30 v/v)) as a function of pH. Percentages are referred to total concentration of L⁴⁻. Charges are omitted.

carboxylate group. The value of first protonation constant derived from the potentiometric titrations was kept constant in this fitting. In order to have a reference, solutions of oxamic acid were titrated with NaOH in the same experimental conditions obtaining values of 1.52(3) and 11.77(2) for pK_{a1} and pK_{a2}, respectively. As one can see, the values of pK_{a1} for the H₄L species and oxamic acid are quite close.

The two last deprotonation constants of the H₄L species could not be determined by potentiometry because, as described in previous works, values of pH greater than 11.0 are required to deprotonate the oxamide group of the *N*-substituted oxamides/oxamates, this weak acidity precluding their evaluation by this technique [25]. However, in the presence of copper(II), deprotonation of the oxamides/oxamates to form the corresponding complex anions takes place at a much lower pH range, allowing their potentiometric determination [26,27–31]. Regarding the formation of the copper(II) complexes in solution, on a first approach, the speciation studies carried out suggested the formation of complexes with a 1:1 metal to ligand stoichiometry. However, since X-ray studies on single crystals revealed the existence of the discrete [Cu₂(H₂L)₂]²⁺·2EtOH and (n-Bu₄N)₂[Cu₂L^{gauche}]⁻·4H₂O dinuclear complexes [17], we performed high resolution ESI mass spectrometry measurements to ascertain the nuclearity of the species existing in solution. The results at pH 5.0 show the presence in solution of the 2:2 copper(II) to ligand species, denoted by *m/z* peaks at 835.0336 and 852.0336, which correspond to the [Cu₂(H₂L)₂ + H]⁺ and [Cu₂(H₂L)₂ + NH₄]⁺ ions, together with the 1:1 species denoted by the *m/z* peak at 435.0470 that can be assigned to the [Cu(H₂L) + NH₄]⁺ ions. A very good agreement between simulated and experimental isotopic distributions was obtained in all cases (see Figs. S2–S4, ESI). Using all this information, a model was proposed and the potentiometric titration data were fitted, obtaining the values grouped in Table 1. One can see therein the formation of one 1:1 metal to ligand mononuclear species and four 2:2 dinuclear complexes with different protonation degrees.

As pointed out above, the oxamic groups become much more acidic in the presence of copper(II) ions. This is illustrated by the distribution diagram shown in Fig. 1 where one can see that the deprotonation of such groups starts already at pH above 5.0 when the [Cu₂(HL)₂]²⁻ species appears. The [Cu₂L₂]⁴⁻ species where all the oxamide groups are deprotonated, prevails in solution above pH ca. 9.5. A rough estimate of the equilibrium constant for the formation of this species through the equation 2L⁴⁻ + 2Cu²⁺ ⇌ [Cu₂L₂]⁴⁻ can be obtained ($\log \beta \sim 29.8$) by considering two times the value of pK_{a2} of the oxamic acid [$pK_{a2} = 11.77(2)$] as the approximate cost for the full deprotonation of H₂L²⁻. The great value of this stability

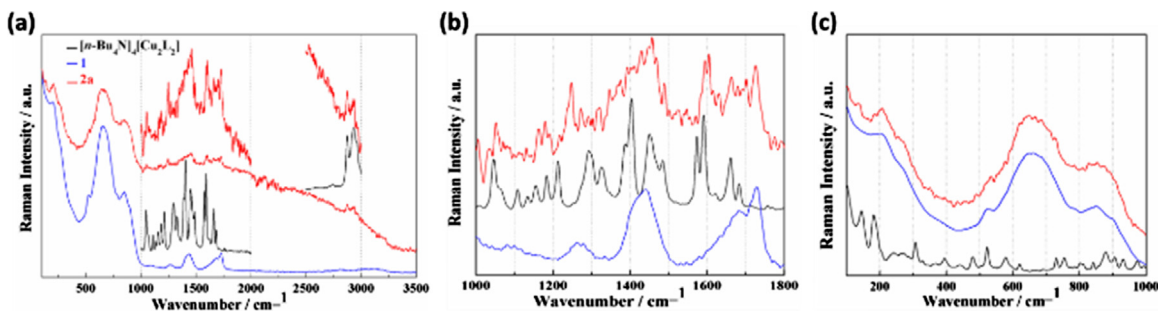


Fig. 2. (a) Full scale FT-Raman spectra of $(n\text{-Bu}_4\text{N})_4[\text{Cu}_2\text{L}_2]$ (black line), **1** (blue line) and **2a** (red line) in the wavenumber range $100\text{--}3500\text{ cm}^{-1}$. The spectrum of $(n\text{-Bu}_4\text{N})_4[\text{Cu}_2\text{L}_2]$ was plotted only in the regions where the related bands are present in the spectrum of the hybrid sample. It is worth emphasizing that some regions have been enlarged to make easier the visualization. FT-Raman spectra of $(n\text{-Bu}_4\text{N})_4[\text{Cu}_2\text{L}_2]$, **1** and **2a** from $1000\text{--}1800\text{ cm}^{-1}$ (b) and (c) $100\text{--}1000\text{ cm}^{-1}$ of $(n\text{-Bu}_4\text{N})_4[\text{Cu}_2\text{L}_2]$, **1** and **2a**. (For interpretation of the references to colour in this figure legend, the reader is referred to the web version of this article.)

constant reveals that this ligand exhibits a high selectivity for the copper(II) ion in respect to other divalent first row transition metal ions, a feature which was already observed in previous reports concerning solution studies with *N*-substituted oxamic acid derivatives and *N,N'*-substituted oxamides [25–31].

These preliminary studies in homogeneous solution are very important to understand which copper(II) species is present on the surface of the niobium(V) oxyhydroxide at each pH value resulting in the formation of the versatile heterogeneous hybrid catalyst.

3.2. Characterization of the hybrid catalyst

The hybrid catalyst **2a** was characterized by X-ray powder diffraction (XPRD), thermal study (TG/DTA), transmission electron microscopy (TEM), scanning electron microscopy (SEM), FTIR and FT-Raman spectroscopy. All the results were compared with the pristine catalyst **1**. The comparison between their X-ray patterns shows new peaks at 14.3 and 22.9° for **2a** that are related to the presence of the dicopper(II) complex in the hybrid material (see Fig. S5, ESI).

The TGA/DTA curves for **1** and **2a** were conducted under a N_2 flow (see Fig. S6, ESI). The TGA curves of both samples show a continuous loss of water molecules until $130\text{ }^\circ\text{C}$ (9.0 and 10.1% for **1** and **2a**, respectively). The thermodecomposition of the hydroxyl groups at the surface of the $\text{NbO}_2(\text{OH})$ matrix for **1** and **2a** occurs in the temperature range $130\text{--}500\text{ }^\circ\text{C}$ concomitantly with the decomposition of the organic ligand in **2a**. These decomposition processes led well-resolved exothermic peaks in the DTA curves.

FT-Raman spectra of $(n\text{-Bu}_4\text{N})_4[\text{Cu}_2\text{L}_2]$, **1** and **2a** (Fig. 2) were carried out in the range $100\text{--}3500\text{ cm}^{-1}$. The comparison between all spectra shows the increase of the number of bands in agreement with the trend of the crystallinity the compounds, **1** < **2a** < $(n\text{-Bu}_4\text{N})_4[\text{Cu}_2\text{L}_2]$ as expected given the slightly amorphous character of **1** and the high crystallinity of **2a**. The main differences between the spectra can be visualized in Fig. 2b. It can be noticed that several bands concerning the C=O and C=C stretching vibrations of $(n\text{-Bu}_4\text{N})_4[\text{Cu}_2\text{L}_2]$ related to **2a** are shifted towards higher wavenumbers, a feature which indicates that the interaction between $(n\text{-Bu}_4\text{N})_4[\text{Cu}_2\text{L}_2]$ and **1** in the hybrid material involves mainly the carbonyl groups and aromatic rings from the ligand counterpart.

The tentative assignment of the main shifts in the FT-Raman spectra of $(n\text{-Bu}_4\text{N})_4[\text{Cu}_2\text{L}_2]$, **1** and **2a** can be found in Table S1. The analysis of the FT-Raman spectrum of the $\text{NbO}_2(\text{OH})$ support in the wavenumber range $2000\text{--}3000\text{ cm}^{-1}$ also suggests that an interaction occurs between the $(n\text{-Bu}_4\text{N})_4[\text{Cu}_2\text{L}_2]$ and **1** in the hybrid material since vibrations attributed to the C-H groups in $(n\text{-Bu}_4\text{N})_4[\text{Cu}_2\text{L}_2]$ are present in **2a**. Yet the major vibrational bands for niobium(V) oxyhydroxide are observed at wavenumber values

lower than 1000 cm^{-1} (Fig. 2c). The position and relative intensities of the bands are dependent on the order, magnitude and Nb-O bonding type. In fact, niobium(V) derivatives with an octahedral NbO_6 surrounding exhibit several vibrational bands related to O-Nb-O bonding in the region $100\text{--}300\text{ cm}^{-1}$ while additional bands located between 500 and 850 cm^{-1} arise from distortions of the ideal octahedral geometry (axial elongation of the O-Nb-O bonds and metal displacement from the mean equatorial plane) [25–34].

The observed changes in the position of these bands in the spectrum of **2a** compared to that of **1** suggest the occurrence of structural distortions in the NbO_6 chromophore after the incorporation of the copper(II) complex. The main changes in the spectrum of **2a** compared to that of **1** are a broadening of the characteristic Nb-O bands (from 500 to 1000 cm^{-1}) together with a decrease in their relative intensities of the characteristic bands related to the Nb-O bond. The modifications observed in the band at 838 cm^{-1} support strong deformations of the Nb-O bonds located on the surface, while the downshift of the band from 662 (1) to 643 cm^{-1} (**2a**) also indicates changes at the bulk level [32–37].

The FTIR spectrum of **2a** (see Fig. S7, ESI) shows closer similarities to that of **1** than the one of $(n\text{-Bu}_4\text{N})_4[\text{Cu}_2\text{L}_2]$. However, the spectrum of **2a** exhibits some shifts of the stretching vibrations in the higher wavenumber region when compared to that of **1** such as $\nu_{\text{O-H}}$ from 3400 and 3014 cm^{-1} (**1**) to 3422 and 3018 cm^{-1} (**2a**) and, $\nu_{\text{C=O}}$ from 1684 and 1720 cm^{-1} (**1**) to 1720 and 1694 cm^{-1} (**2a**). The peak located at 1268 cm^{-1} in the spectrum of **2a** is tentatively attributed to the angular deformation of the C-H bond from the aromatic ring of the ligand counterpart. In the lower wavenumber region, the absorption peak centred at 750 cm^{-1} of **2a** ($\delta_{\text{C-C}}$ bending vibration), is shifted to the higher frequency region compared to the corresponding band in the spectrum of **1** (ca. 624 cm^{-1}).

The formation of **1** and the incorporation of the complex $(n\text{-Bu}_4\text{N})_4[\text{Cu}_2\text{L}_2]$ into its matrix to obtain **2a** was monitored through the analysis of the deconvolution bands in their FTIR spectra in the region $3700\text{--}2600\text{ cm}^{-1}$ (see Fig. S8, ESI).

These bands are related to the stretching vibrations of the O-H bonds located at 3100 cm^{-1} revealing the presence of internal hydroxo groups from the bulk. In fact, the $\nu_{\text{O-H}}$ stretchings at 3450 cm^{-1} are equivalent to the hydroxo groups present on the surface, as reported by Cornell and Schwertmann [32]. In addition, the hybrid catalyst **2a** exhibits a shift from 3438 cm^{-1} to 3570 cm^{-1} , obtained by the Gaussian adjust, that suggests thus a modification on the surface of the support **1**.

Typical scanning electron micrographs for **2a** (Figs. 3a and 3d) show several changes in the $\text{NbO}_2(\text{OH})$ support induced by the adsorption of the $[\text{Cu}_2\text{L}_2]^{4-}$ complex on its surface, accordingly with the preparation method used. The differences with the pristine $\text{NbO}_2(\text{OH})$ support (see Fig. S9, ESI) are associated with the texture

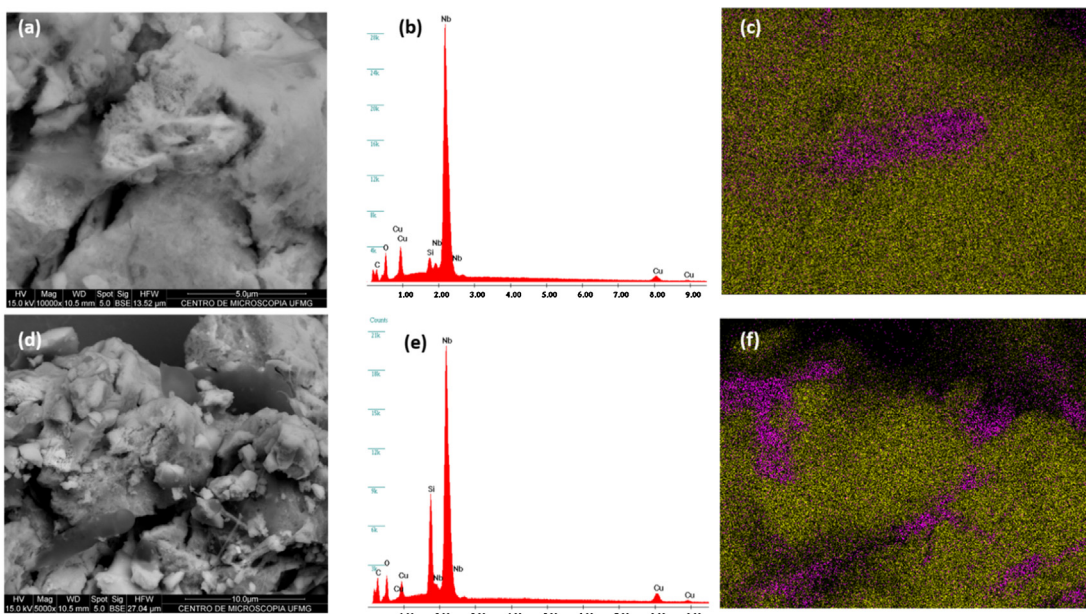


Fig. 3. Compilation of SEM images [(a) and (d)] with the EDS analyses [(b) and (e)] and SEM element mapping [(c) and (f)] for **2a**. Yellow and pink dots at the SEM element mapping represent the Nb and Cu distributions, respectively. (For interpretation of the references to colour in this figure legend, the reader is referred to the web version of this article.)

of the hybrid material, an amorphous phase being observed in **2a** which covers part of the material. We conclude that most likely, this amorphous phase is a copper-containing aggregate, since the SEM element mapping (Figs. 3c and f) corroborates the EDS analyses (Figs. 3b and e), showing the presence of copper in the spectra. In order to verify that the amorphous

phase actually represents the copper(II) complex instead of a copper oxide, we observed the mapping of carbon, which shows a similarity with the copper region (see Fig. S10, ESI) characterizing thus the presence of the organic ligand. It is worth to emphasize that not necessarily the copper(II) complex is non-homogeneously dispersed, since the resolution of the analyzer does not allow us to observe thin films of the copper(II) complex covering the $\text{NbO}_2(\text{OH})$ platelets.

The TEM images of **1** and **2a** are very similar (see Fig. S11, ESI), as expected because of the copper(II) complex is well dispersed into the oxyhydroxide matrix. In addition, agglomeration spots which are commonly attributed to metals, alloys or copper oxides [38] were not observed in the micrographs.

The textural characteristics of the hybrid **2a** were also inferred from the N_2 adsorption/desorption experiments. The isotherms for **1** and **2a** are shown in Fig. S12 (ESI). The calculated specific surface areas are 7 and $2 \text{ m}^2 \text{ g}^{-1}$ for **1** and **2a** respectively, values which are very low as expected from the comparison of their isotherm curves with those previously described in the literature [12].

3.3. Catalytic tests

Finally, in order to test the effect of the copper(II) complex anchored over the surface of the niobium oxyhydroxide, oxidation reactions of the methylene blue dye (MB) were performed in the presence of H_2O_2 (Fenton-like reaction). The MB dye is a model substrate which is commonly used to evaluate the potential application of a new catalyst in oxidation reactions to mineralize pollutants from an aqueous effluent.

Fenton-like reactions were performed using solutions containing 100 ppm of the MB dye and 1000 ppm of the DBT in *n*-hexane in the presence of H_2O_2 . The MB dye and the DBT are model substrates, which are commonly used to evaluate the potential application of

catalyst in oxidation reactions to mineralize pollutants from heavier fractions of petroleum.

The profile of the oxidation kinetics for the MB dye is shown in Fig. 4a. The catalyst **2a** exhibits different profiles in acidic and basic media, being more effective in the decomposition of the dye in basic media (pH value of 12.0) in the first 30 min, reaching up to 75% of discoloration, as monitored by UV-vis measurements. Less than 50% of the MB dye was oxidized in the first 30 min under pH values of 2.0 and 5.5. However, the amount of oxidized organic matter achieves 80% after reacting for 60 min, in both basic and acid media.

These results indicate that the copper(II) complex can undergo conformational changes at different values of pH, while remaining anchored to the surface of **1**, as illustrated by Scheme 2. In the structure of the $[\text{Cu}_2\text{L}_2]^{4-}$ species present in **2a**, each copper(II) ion has a distorted square planar geometry in which each oxamate group of the L^{4-} ligand acts in a chelating mode through one carboxylate-oxygen and the amidate-nitrogen. On the other hand, each copper centre in the $[\text{Cu}_2(\text{H}_2\text{L})_2]$ complex is six-coordinate, the two monoprotonated oxamate groups of each H_2L^{2-} ligand adopting the bidentate/monodentate binding mode and a molecule of solvent occupying one axial position. This difference is due to the protonation of the nitrogen atoms of the two amide groups in H_2L^{2-} , a feature which prevents their coordination in acidic media. In addition, the copper(II) complex in the hybrid catalyst **2a** assumes a conformation at higher pH values that exposes more effectively the copper(II) sites, making more efficient its reaction with hydrogen peroxide and the resulting hydroxyl radical.

The study of the kinetics of the MB dye removal at pH 12.0 was performed by considering both the hybrid catalyst **2a** and the support **1** for comparison (Fig. 4b). The catalyst **2a** showed approximately 80% of MB dye removal after 30 min of reaction. On the other hand, the removal capacity observed for the niobium(V) oxyhydroxide in the lack of the dicopper(II) complex was only 55%. This result illustrates the positive role played by the $(n\text{-Bu}_4\text{N})_4[\text{Cu}_2\text{L}_2]$ complex anchored over the niobium(V) oxyhydroxide support, enhancing its catalytic activity in a Fenton-like oxidation reaction.

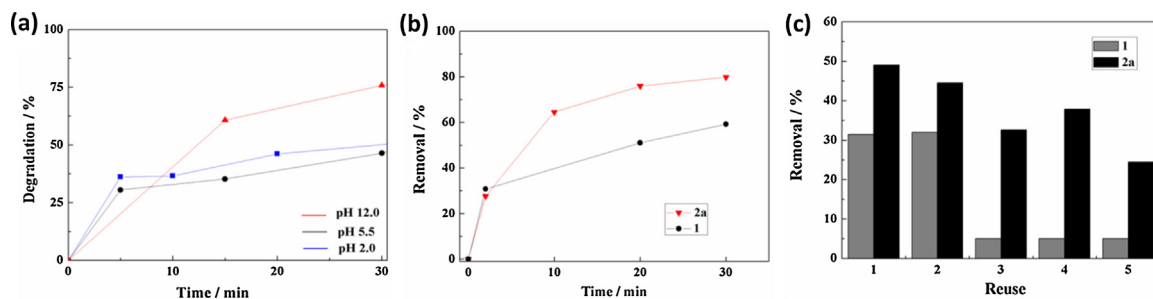
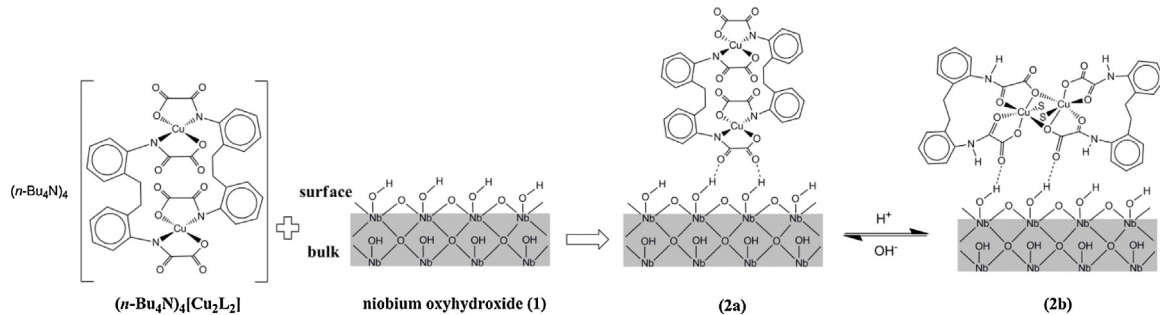


Fig. 4. (a) Catalytic degradation of the MB dye using **2a** and the Fenton-like reaction at pH values of 2.0, 5.5 and 12.0 in the darkness. (b) Kinetics of the removal of the MB dye at a pH value of 12.0 from the hybrid compound **2a** and the support **1**. (c) Reuse cycles with the catalyst **1** (grey) and the hybrid catalyst **2a** (black); both of them were analyzed in MB dye for 30 min at the concentration of 100 ppm.



Scheme 2. Preparation of the catalyst **2a** starting from the pristine $\text{NbO}_2(\text{OH})$ and the dicopper(II) complex $(n\text{-Bu}_4\text{N})_4[\text{Cu}_2\text{L}_2]$ plus the acid-base equilibrium involving the niobium(V) oxyhydroxide and the complex grafted on its surface. It is worth nothing that the conformation of the dicopper(II) complex changes in the structures **2a** and **2b** depending on the pH value [17].

Reuse of both catalysts **1** and **2a** was performed five times, as shown in Fig. 4c. The catalytic activity of **1** strongly decreases a lot after the third cycle. On the contrary, **2a** presents a better activity for reuse than **1**. These results suggest the improvement in the ability of the hybrid catalyst **2a** towards the decomposition of the pollutant in sequential reactions when compared with the catalyst **1**. Again, the copper(II) complex may be responsible for the better performance of the hybrid catalyst for reuse.

In order to demonstrate the formation of putative intermediates in the Fenton-like oxidation reaction, which may indicate the catalytic action by hydroxyl radical generation, the solutions were analyzed by ESI(+)-MS (see Fig. S13, ESI) and the peak referent to the molecular ion MB m/z 284 was monitored. Before the reaction, a signal related to the MB dye structure could be observed. After 30 min, the reaction employing the catalyst **1** shows the appearance of signals at m/z = 300, 318, 334 and 362 corresponding to the hydroxylation of the MB dye structure. Moreover, the occurrence of additional signals at m/z = 218 and 149, values which are smaller than the one of m/z = 284 corresponding to the remaining dye, suggests a further MB degradation.

In the presence of the hybrid catalyst **2a**, a greater degradation capacity of the MB dye can be seen leading to a complete disappearance of the signal m/z = 284. These results corroborate the aforementioned kinetics and reuse data, and confirm the catalytic effect of the dicopper(II) complex in the hybrid catalyst **2a** (Fig. 4).

Fenton-like reactions for the DBT using the hybrid catalyst **2a** were investigated under three different radiations: UV, visible and ambient lights. The absorption of DBT was monitored through UV-vis at $\lambda_{\text{max}} = 236 \text{ nm}$ after 60 min of reaction. The removal range of DBT was 28–36% (see Fig. 5). The experiment conducted in visible light presented the lowest removal of 28% while the highest removal of 36% was at the ambient light. The removal of 32% was obtained in the UV light. Those results show no dependence between the degradation of DBT and the energy of the incident

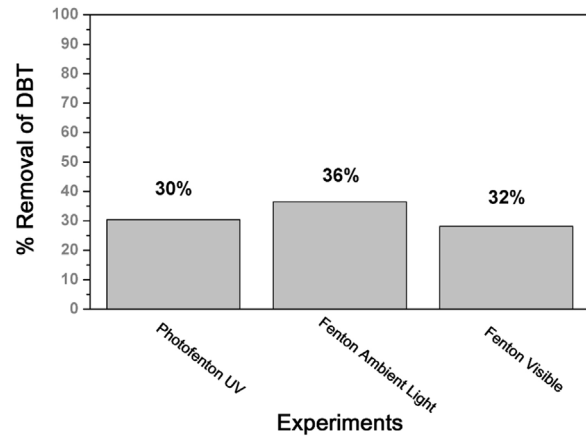


Fig. 5. Percentage of DBT degradation. Conditions: 0.010 g of **2a** in 10 mL of 1000 ppm DBT in *n*-hexane.

light. The presence of H_2O_2 was the only determining factor for the DBT removal.

4. Conclusions

The preparation and characterization of coordination compounds and their association with heterogeneous catalysts to produce hybrid catalysts have undergone a fast development in the last years. An impressive growth in the number of sophisticated supramolecular materials obtained by means of coordination chemistry envisaging the environmental catalysis provides new opportunities in tuning the properties of classical metal oxides. In this contribution, we present a new example of improvement of the activity of the well-known catalyst $\text{NbO}_2(\text{OH})$ (**1**) towards

the decomposition of the MB dye both in acid and basic media. Furthermore, the hybrid catalyst $\text{NbO}_2(\text{OH})\text{-}[\text{Cu}_2\text{L}_2]$ (**2a**) can be reused for at least five times without losing its catalytic performance in contrast to the case of **1**.

Notwithstanding, some aspects remain still unexplored concerning this hybrid system such as the comprehension of the catalytic mechanism at the molecular level and the extension to other reaction types. Therefore, we think that the field of the supramolecular environmental catalysis can bring several advances in the domains of sustainable development, green chemistry and synthesis of fine chemical products.

Acknowledgements

This work was supported by the CAPES, CNPq, FAPEMIG (Brazil), MICINN (Spain) (Projects CTQ-2013-44844P and Unidad de Excelencia María de Maeztu MDM-2015-0538), the Generalitat Valenciana (PROMETEO II/2015/002) and the Brazilian-Spanish Project HB2014-00024.

Appendix A. Supplementary data

Supplementary data associated with this article can be found, in the online version, at <http://dx.doi.org/10.1016/j.apcatb.2017.01.086>.

References

- [1] M.F. Ashby, Y.J.M. Bréchet, *Acta Mater.* 51 (2003) 5801–5821.
- [2] L.F. Giraldo, B.L. López, L. Pérez, S. Urrego, L. Sierra, M. Mesa, *Macromol. Symp.* 258 (2007) 129–141.
- [3] O. Deutschmann, H. Knözinger, K. Kochloefl, T. Turek, *Ullmann's Encyclopedia of Industrial Chemistry*, Wiley-VCH Verlag GmbH & Co. KGaA, 2000.
- [4] J.C. Rooke, T. Barakat, J. Brunet, Y. Li, M.F. Finol, J.-F. Lamonier, J.-M. Giraudon, R. Cousin, S. Siffert, B.L. Su, *Appl. Catal. B: Environ.* 162 (2015) 300–309.
- [5] Y. Li, S. Yan, L. Qian, W. Yang, Z. Xie, Q. Chen, B. Yue, H. He, *J. Catal.* 241 (2006) 173–179.
- [6] M. Paulis, M. Martín, D.B. Soria, A. Díaz, J.A. Odriozola, M. Montes, *Appl. Catal. A: Gen.* 180 (1999) 411–420.
- [7] S. Furukawa, A. Tamura, T. Shishido, K. Teramura, T. Tanaka, *Appl. Catal. B: Environ.* 110 (2011) 216–220.
- [8] Departamento Nacional de Produção Mineral (DNPM), *Journal* 141 (2014).
- [9] I. Nowak, M. Ziolek, *Chem. Rev.* 99 (1999) 3603–3624.
- [10] Z.-L. Wang, H.-Q. Tan, W.-L. Chen, Y.-G. Li, E.-B. Wang, *Dalton Trans.* 41 (2012) 9882–9884.
- [11] T.L. Gianetti, R.G. Bergman, J. Arnold, *Chem. Sci.* 5 (2014) 2517–2524.
- [12] L.C.A. Oliveira, M.F. Portilho, A.C. Silva, H.A. Taroco, P.P. Souza, *Appl. Catal. B* 117–118 (2012) 29–35.
- [13] P. Chagas, H.S. Oliveira, R. Mambrini, M. Le Hyaric, M.V. De Almeida, L.C.A. Oliveira, *Appl. Catal. A Gen.* 454 (2013) 88–92.
- [14] T.E. Souza, M.F. Portilho, P.M.T.G. Souza, P.P. Souza, L.C.A. Oliveira, *ChemCatChem* 6 (2014) 2961–2969.
- [15] L.C.A. Oliveira, A.C. Silva, M.C. Pereira, *RSC Adv.* 5 (2015) 44567–44570.
- [16] M. Barboiu, *Eur. J. Inorg. Chem.* 2015 (2015) 1112–1125.
- [17] W.D. do Pim, W.X.C. Oliveira, M.A. Ribeiro, E.N. de Faria, I.F. Teixeira, H.O. Stumpf, R.M. Lago, C.L.M. Pereira, C.B. Pinheiro, J.C.D. Figueiredo-Junior, W.C. Nunes, P.P. de Souza, E.F. Pedroso, M. Castellano, J. Cano, M. Julve, *Chem. Commun.* 49 (2013) 10778–10780.
- [18] W.D. do Pim, T.R.G. Simoes, W.X.C. Oliveira, I.R.A. Fernandes, C.B. Pinheiro, F. Lloret, M. Julve, H.O. Stumpf, C.L.M. Pereira, *Cryst. Growth Des.* 14 (2014) 5929–5937.
- [19] E. Garcia-España, M.-J. Ballester, F. Lloret, J.M. Moratal, J. Faus, A. Bianchi, *J. Chem. Soc. Dalton Trans.* 1 (1988) 101–104.
- [20] M. Fontanelli, M. Micheloni, Presented in Part at the First Spanish-Italian Congress on Thermodynamics of Metal Complexes, Diputación De Castellón, Spain, 1990.
- [21] G. Gran, *Analyst* 77 (1952) 661–671.
- [22] F.J.C. Rossotti, H. Rossotti, *J. Chem. Educ.* 42 (1965) 375–378.
- [23] A. Avdeef, K.J. Box, J.E.A. Comer, M. Gilges, M. Handley, C. Hibbert, W. Patterson, K.Y. Tam, *J. Pharmac. Biomed. Anal.* 20 (1999) 631–641.
- [24] P. Gans, A. Sabatini, A. Vacca, *Talanta* 43 (1996) 1739–1753.
- [25] R. Ruiz, J. Faus, F. Lloret, M. Julve, Y. Journaux, *Coord. Chem. Rev.* 193–195 (1999) 1069–1117.
- [26] T.S. Fernandes, R.S. Vilela, A.K. Valdo, F.T. Martins, E. García-España, M. Inclán, J. Cano, F. Lloret, M. Julve, H.O. Stumpf, D. Cangussu, *Inorg. Chem.* 55 (2016) 2390–2401.
- [27] F. Lloret, M. Julve, J. Faus, Y. Journaux, M. Philoche-Levisalles, Y. Jeannin, *Inorg. Chem.* 28 (1989) 3702–3706.
- [28] F. Lloret, J. Sletten, R. Ruiz, M. Julve, J. Faus, M. Verdaguer, *Inorg. Chem.* 31 (1992) 778–784.
- [29] F. Lloret, M. Julve, J. Faus, R. Ruiz, I. Castro, M. Mollar, M. Philoche-Levisalles, *Inorg. Chem.* 31 (1992) 784–791.
- [30] F. Lloret, M. Julve, J.A. Real, J. Faus, R. Ruiz, M. Mollar, I. Castro, C. Bois, *Inorg. Chem.* 31 (1992) 2956–2961.
- [31] J.A. Real, M. Mollar, R. Ruiz, J. Faus, F. Lloret, M. Julve, M. Philoche-Levisalles, *J. Chem. Soc. Dalton Trans.* (1993) 1483–1488.
- [32] R.M. Cornell, U. Shwertman, *The Iron Oxides: Structure, Properties, Reactions, Occurrences and Uses*, VCH, New York, 1996.
- [33] J.-M. Jehng, I.E. Wachs, *Catal. Today* 8 (1990) 37–55.
- [34] A.A. McConnell, J.S. Aderson, C.N.R. Rao, *Spectrochim. Acta Part A: Mol. Spectrosc.* 32 (1976) 1067–1076.
- [35] D. Stošić, S. Bennici, V. Rakić, A. Auroux, *Catal. Today* 192 (2012) 160–168.
- [36] I.E. Wachs, J.M. Jehng, G. Deo, H. Hu, N. Arora, *Catal. Today* 28 (1996) 199–205.
- [37] X. Gao, S.R. Bare, B.M. Weckhuysen, I.E. Wachs, *J. Phys. Chem. B* 102 (1998) 10842–10852.
- [38] D. Walsh, L. Arcelli, T. Ikoma, J. Tanaka, S. Mann, *Nat. Mater.* 2 (2003) 386–390.